Int J Cardiovasc Imaging (2017) 33:1021–1031
DOI 10.1007/s10554-017-1084-4

ORIGINAL PAPER

Myocardial perfusion imaging with PET

Roel S. Driessen[1] · Pieter G. Raijmakers[2] · Wijnand J. Stuijfzand[1] · Paul Knaapen[1]

Received: 19 September 2016 / Accepted: 27 January 2017 / Published online: 10 February 2017

Abstract Noninvasive assessment of coronary artery disease remains a challenging task, with a large armamentarium of diagnostic modalities. Myocardial perfusion imaging (MPI) is widely used for this purpose whereby cardiac positron emission tomography (PET) is considered the gold standard. Next to relative radiotracer distribution, PET allows for measurement of absolute myocardial blood flow. This quantification of perfusion improves diagnostic accuracy and prognostic value. Cardiac hybrid imaging relies on the fusion of anatomical and functional imaging using coronary computed tomography angiography and MPI, respectively, and provides incremental value as compared with either stand-alone modality.

Keywords Myocardial perfusion imaging · Positron emission tomography · Myocardial blood flow

Introduction

Positron emission tomography (PET) is a radionuclide imaging technique that allows for noninvasive quantification of myocardial blood flow (MBF) in vivo. Assessment of myocardial perfusion provides important diagnostic and prognostic information for suspected or known coronary artery disease (CAD). Due to its limited availability, methodologic complexity, and high cost, cardiac PET has long been considered to be a research tool only. In recent years, however, PET technology has been fused with computed tomography (CT). These hybrid devices have gained great popularity, predominantly driven by their success in clinical oncology, which has led to an exponential growth of the numbers of scanners installed worldwide. This growth in hardware has been paralleled by improvements in radiotracer availability and advances in postprocessing software. Consequently, cardiac PET has witnessed more widespread use and routine implementation in clinical practice. This review will outline the fundamental principles of cardiac PET imaging and available tracer characteristics. Subsequently, clinical implications of myocardial perfusion imaging (MPI) will be delineated with special emphasis on quantification of MBF and the additive value of hybrid PET/CT imaging.

Principles of PET

PET relies on the simultaneous detection of two photons, emitted from the decay of radionuclide tracers. In more detail, positrons are emitted during the distribution of these tracers in the patient's body and collide with an electron. Consequently, a positron annihilates, which results in the emission of two photons in opposite directions. Since the average range traveled by positrons is small, in the order of mm, the decay can be considered to have occurred along the straight line described by the two annihilation photons. A PET scanner contains several rings of detectors, made of a scintillating material, which convert the energy of the annihilation photons proportionally into an electrical signal. Two photons are considered to have been emitted simultaneously when they are detected within the narrow coincidence-timing window of the scanner, around 6–12 ns.

✉ Paul Knaapen
p.knaapen@vumc.nl

1 Department of Cardiology, VU University Medical Center, De Boelelaan 1117, 1081 HV Amsterdam, The Netherlands

2 Department of Nuclear Medicine and Radiology, VU University Medical Center, Amsterdam, The Netherlands

Accordingly, when two photons are detected simultaneously, a decay event should have occurred somewhere along the line between two detectors. By detection of these annihilation photon pairs, the distribution of the positron-emitting nuclides in the patients part positioned within the field-of-view of the PET scanner can be reconstructed.

PET versus SPECT

As compared with single-photon emission computed tomography (SPECT), PET has several advantages. One of the main benefits is the superior image quality of PET over SPECT. This improvement is due to more favorable tracer characteristics, improved count statistics, as well as the routine and more accurate application of photon attenuation correction (AC). Although this correction technique is increasingly available for SPECT imaging with possible benefit in terms of diagnostic accuracy, the downside is that it can also induce artifacts [1]. Furthermore, smaller and more subtle perfusion defects can be detected due to higher spatial resolution of PET (typically 4–7 mm) as compared to SPECT (typically 12–15 mm). Next to spatial resolution, also temporal resolution is in favor of PET, which allows for absolute quantification of perfusion by tracking the dynamic tracer activities of arterial blood and myocardium through time. Although it has been attempted for SPECT [2], PET is an established tool to provide clinically relevant quantitative levels of perfusion and flow reserve next to qualitative myocardial perfusion images [3–6]. Other advantages include a lower radiation burden and acquiring both rest and stress images within a single scanning session due to the short physical half-life of the PET perfusion tracers. The main limitation for PET is the need for an on-site cyclotron or generator with the current tracer agents as will be discussed in more detail. An overview of PET and SPECT imaging characteristics are provided in Table 1.

Table 1 SPECT and PET characteristics

	SPECT	PET
Availability	Wide	Limited
Attenuation correction	Less accurate	Accurate
Spatial resolution	12–15 mm	4–7 mm
Protocol	1–2 days	<1 h
Radiation	>5 mSv	<5 mSv
Images	Qualitative	Quantitative
Hybrid with CT	Yes	Yes

SPECT single-photon emission computed tomography; *PET* positron emission tomography; *mSv* millisievert

Perfusion tracer characteristics

Of several available PET tracers, ^{82}Rb, $^{13}NH_3$, and $H_2{}^{15}O$ are the most commonly used for the assessment of myocardial perfusion [3]. Additionally, ^{18}F-flurpiridaz is an emerging perfusion tracer which holds great clinical potential but is not yet available for clinical use and is currently being tested in phase 3 trials [7–9]. Tracer specific characteristics, including pros and cons, will be described below and summarized in Table 2. It's important to realize that none of the perfusion tracers excels on all of these features. Therefore the choice of tracer is multifactorial and depending on practical considerations, as well as the aim of the PET imaging program.

Table 2 PET tracers characteristics

	$H_2{}^{15}O$	$^{13}NH_3$	^{82}Rb	^{18}F-flurpiridaz
Half-life	123 s	9.97 min	76 s	110 min
Production	Cyclotron	Cyclotron	Generator	Cyclotron
Kinetics	Freely diffusible, metabolically inert	Metabolically trapped in myocardium	Metabolically trapped in myocardium	Metabolically trapped in myocardium
Mean positron range in tissue	1.1 mm	0.4 mm	2.8 mm	0.2 mm
Data acquisition	Dynamic	Dynamic, static	Dynamic, static	Dynamic, static
Scan duration	6 min	20 min	6 min	20 min
Gating/LV function	−	+	+	+
Radiation dose	~0.4 mSv	~1 mSv	~3 mSv	~4 mSv
Quantification	Excellent	Good	Moderate	Very good
Image quality	Good (parametric images)	Very good	Good	Excellent

$H_2{}^{15}O$, oxygen-15-labeled water, $^{13}NH_3$, 13 N-labeled ammonia; ^{82}Rb, ^{82}rubidium; LV, left ventricular; other abbreviations as in Table 1

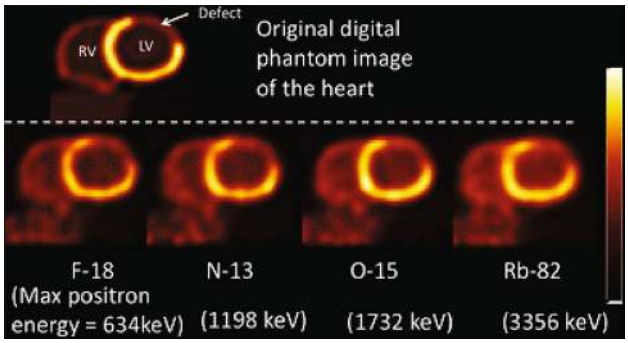

Fig. 1 Simulated short-axis images using digital cardio-torso phantom for different positron emitting radioisotopes (^{18}F, ^{13}N, ^{15}O and ^{82}Rb). Blurring effect by positron range increases with higher positron kinetic energy. Adapted from Rischpler et al. [8]

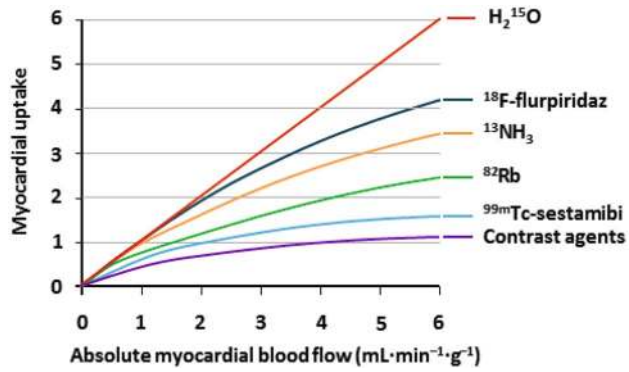

Fig. 2 Kinetics of myocardial perfusion tracers and contrast agent. Graphical presentation of the relationship between absolute myocardial blood flow and tracer uptake for currently available PET radiotracers and ^{18}F-flurpiridaz, which is not yet available for clinical use. Also included are the kinetics of the commonly used SPECT radiotracer (^{99m}Tc-Sestamibi) as well as contrast agents for CT and CMR perfusion (i.e. iodine and gadolinium based contrast agent). Adapted from Danad et al. [30]

Among clinically used perfusion tracers, $H_2{}^{15}O$ features fundamentally different properties compared to ^{82}Rb, $^{13}NH_3$, and ^{18}F-flurpiridaz [3, 6, 10]. Namely, ^{82}Rb is a potassium analog and is taken up by myocardial cells via the Na/K ATP transporter in a rapid and active manner [11]. While $^{13}NH_3$ is incorporated into the glutamine pool through active transport and passive diffusion processes [12]. ^{18}F-flurpiridaz is derived from pyridazinone and binds avidly to mitochondrial complex-1 [13]. In other words, these three tracers are transported across the cell membrane and effectively become metabolically trapped while they are cleared from the intravascular compartment (arterial blood pool). Consequently, 'late' static uptake images of these tracers account for high tissue-to-background ratios and result in excellent qualitative grading of relative perfusion distribution. The combination of these images with ECG-gating permits the assessment of left ventricular (LV) volumes and function as well as regional wall motion [14].

In contrast, $H_2{}^{15}O$ diffuses freely across myocyte membranes, is metabolically inert and thereby promptly reaching equilibrium between blood and tissue without accumulation in the myocardium. As a consequence, radiotracer distribution images of $H_2{}^{15}O$ are of poor image quality and provide little diagnostic value. The lack of diagnostic images has long prohibited the use of $H_2{}^{15}O$ in clinical practice and nearly all studies on qualitative imaging for CAD have been conducted with ^{82}Rb or $^{13}NH_3$ [15]. In recent years, however, digital subtraction techniques and parametric imaging by automated software packages now generate qualitative gradable images that display perfusion at a voxel level, based on the tracer kinetic model for each voxel [16, 17]. These images are distinctly different from actual tracer uptake images as they represent a graphical illustration of quantitative flow values. These developments have enabled $H_2{}^{15}O$ to be utilized in clinical practice [18, 19].

Image quality is additionally determined by the positron range in tissue. High-energy positrons penetrate deeper into tissue before annihilation occurs and demonstrate decreased spatial resolution compared to low-energy positrons. Therefore, image resolution gradually increases from ^{82}Rb, $H_2{}^{15}O$, $^{13}NH_3$, to ^{18}F-flurpiridaz, respectively, according to their energetic state (Fig. 1) [4]. Moreover, the physical half-life of the radioactive compounds determines the potential acquisition duration and therefore count-statistics. The short physical half-life of ^{82}Rb and $H_2{}^{15}O$ allows a timeframe of only a few minutes of acquisition before the tracer is decayed to background levels, whereas $^{13}NH_3$ and ^{18}F-flurpiridaz acquisitions can be continued till satisfactory counts-statistics are obtained, which enhances image quality. These factors result in the highest image quality of ^{18}F-flurpiridaz given its long half-life and low positron range as opposed to relative poor image quality of ^{82}Rb with its ultra-short half-life and high positron range.

Next to relative uptake images, PET enables the assessment of absolute levels of tracer concentration. Using a dynamic acquisition (i.e. multiple frames initiated upon administration of the tracer) time-activity curves can be generated of tracer flux for arterial blood and myocardium. Automated software then computes myocardial blood flow (MBF) in absolute terms (in units of $mL \cdot min^{-1} \cdot g^{-1}$) and calculates coronary flow reserve (CFR) [16, 17]. An ideal tracer for these measurements is characterized by accumulation in/or clearance from myocardium proportionally linear to perfusion, irrespective of flow rate or metabolic state [20]. $H_2{}^{15}O$ is the only tracer that meets these criteria and is considered the

gold standard for quantification of MBF [21]. The other aforementioned tracers have the property that myocardial extraction from arterial blood is incomplete and curvilinear with increasing flow rates, frequently referred to as the "roll-off" phenomenon (Fig. 2) [22]. PET derived MBF measurements are therefore underestimated with increasing actual flow. Correction models based on animal experiments can be employed yet induce noise, particularly when large correction factors are required with severely blunted extraction at high perfusion levels or with tracers characterized by a lower extraction fraction. Nonetheless, each of these tracers has been tested in animal experiments against microsphere-quantified perfusion, the invasive reference standard. $H_2{}^{15}O$ and $^{13}NH_3$ in particular have been well validated and display close agreement with microsphere flow and demonstrate low test–retest variability (10–15%) [10, 21, 23–25]. In recent years, automated software packages have been developed and improved, applying these validated models. Postprocessing is now in the order of minutes, and these packages display high reproducibility [16, 26, 27]. Quantification of ^{82}Rb is less reliable as this tracer harbors intrinsic limitations (ultrashort physical half-life, long positron range, and low extraction fraction). Nonetheless, its extraction fraction is still superior to Technetium-99m (^{99m}Tc)-labeled SPECT (Fig. 2) and recent studies have shown MBF measurements of ^{82}Rb to be feasible [28]. Limited data are available concerning the quantification of ^{18}F-flurpiridaz, but its characteristics and kinetics (very high extraction fraction and short positron range) have the potential for highly reliable perfusion measurements [8, 20, 29].

Of interest, recent developments enabled the estimation of quantitative MBF using alternative noninvasive imaging techniques, such as cardiovascular magnetic resonance imaging (CMR) and CT, with the use of contrast media [31, 32]. The low extraction fraction of these iodine and gadolinium based contrast agents (Fig. 2), however, necessitates the use of extensive corrections and limits the accuracy of MBF measurements.

Tracer production and availability

A fundamental concern for widespread clinical application of cardiac PET perfusion imaging is the necessity to produce the utilized tracers onsite. In this regard, the currently available tracers $H_2{}^{15}O$ and $^{13}NH_3$ require a cyclotron in close proximity of the scanning facilities. Additionally, while $H_2{}^{15}O$ is mainly used in European and Asian nuclear imaging labs at this time, FDA hasn't approved this tracer for clinical use. ^{82}Rb, however, is produced by a $^{82}Sr/^{82}Rb$ generator obviating the need for a cyclotron and is therefore more convenient to implement in clinical practice. The downside of this approach is that the generator needs to be replenished every 28 days at relatively high costs ($20,000). In order to make such a program cost-effective, a high volume patient throughput is needed. These issues may soon be overcome by the emerging fluorine-labeled tracers such as ^{18}F-flurpiridaz [8]. Because its longer physical half-life of 110 min allows for off-site production, this tracer has great potential for widespread implementation. ^{18}F-labeled perfusion tracers also benefit from the fact that they can be used in physical exercise protocols whereby the radioisotope is administered during maximal exertion. ^{82}Rb, $H_2{}^{15}O$, and $^{13}NH_3$ require injection while the patient is lying inside the scanner, as tracer decay is too rapid to transport the patient from the treadmill or stationary bike to the scanner. These tracers can therefore only be utilized in conjunction with pharmacological stressor agents.

Clinical value of myocardial blood flow imaging

Similar to SPECT, in clinical practice PET perfusion images are most commonly graded visually and in a qualitative manner. Relative radiotracer distribution is assessed during both rest and stress (or hyperemic) conditions. Myocardial perfusion defects are usually graded by their extent, severity, and location. Current guidelines recommend a semiquantitative analysis using a segmental 5 point scale system (normal = 0, mild defect = 1, moderate defect = 2, severe defect = 3, and absent uptake = 4) on a 17 segment model of the left ventricle [33, 34]. These scores can be summed for rest (SRS) and stress (SSS) with a subsequent summed difference score (SDS) in order to identify reversibility [35]. Fixed defects are compatible with myocardial scarring or hibernating myocardium, whereas reversibility of stress induced hypoperfusion is compatible with ischemia.

Next to qualitative and semiquantitative grading, PET also allows for absolute quantification of perfusion. Several available automatic software packages routinely provide these MBF values per myocardial territory. Derived MBF values can then be compared with normalcy ranges of flow. Normal databases, however, display a broad base of hyperemic MBF between 2 and 5 mL min^{-1} g^{-1}, which is attributable to variability in minimal microvascular resistance and is dependent on age, sex, and traditional cardiovascular risk factors [36–39]. Currently, still limited data are available with regard to an optimal threshold to distinguish pathological from normal hyperemic MBF and myocardial flow reserve [5]. In addition, thresholds for PET derived MBF values are not interchangeable for different radiotracers. Although in general, a myocardial flow reserve below two is considered abnormal whereas beyond 2.5 is deemed

normal, with an ambiguous transition zone between 2.0 and 2.5 [6]. These values were confirmed by a recent multicenter study presenting an optimal threshold of 2.30 mL min^{-1} g^{-1} for hyperemic MBF and 2.50 mL min^{-1} g^{-1} for myocardial flow reserve when compared with invasive fractional flow reserve (FFR) measurements [40]. It can be questioned, however, whether single thresholds are reasonable. Alternatively, MBF values might be interpreted on a continuous scale for diagnostic and prognostic purposes as well as subsequent clinical decision making [5]. Therefore ongoing studies are targeted to further define the normal limits of (hyperemic) perfusion, especially for different subgroups such as revascularized patients as well as patients with diabetes and cardiomyopathies [41]. Another important issue is that myocardial perfusion imaging reflects the composite of the epicardial as well as the microvascular bed. This means that diminished flow values may originate from either epicardial or microvascular disease, or both.

Diagnostic accuracy of PET imaging

The majority of studies exploring the diagnostic accuracy of PET perfusion imaging for the detection of CAD, have been conducted with static uptake images of ^{82}Rb and $^{13}NH_3$. Compared with SPECT, perfusion imaging using PET consistently yields the highest diagnostic accuracy [42–44]. Sensitivity and specificity for PET in these meta-analyses ranged from 84 to 93% and 81 to 88%, respectively. It must be acknowledged, however, that most of these studies were compared with invasive coronary angiography without FFR and therefore lack an appropriate reference standard.

Diagnostic accuracy testing has been less extensive for quantitative perfusion imaging. Increasing data, however, show the superiority of quantitative assessment over static uptake image grading [45–49]. Typical groups of patients which could benefit the most from quantitative assessment include patients with multivessel disease (i.e. balanced ischemia), early stage blood flow impairment, and microvascular disease [6, 47, 50]. Especially multivessel disease frequently results in false negative interpretation of relative radiotracer uptake, because the myocardial region with the highest uptake is considered the normal reference region. Absolute blood flow quantification would then reveal that this region is abnormally perfused as well. This is illustrated with an example in Fig. 3. Apart from this, the combination with ECG gated derived information such as LV function and transient ischemic dilatation (TID) seems to increase diagnostic accuracy of qualitative uptake images [51, 52].

Another interesting finding from recent studies is that hyperemic MBF quantification outperforms CFR to diagnose obstructive CAD, highlighting the potential of stress only protocols [40, 53, 54]. The largest of these studies,

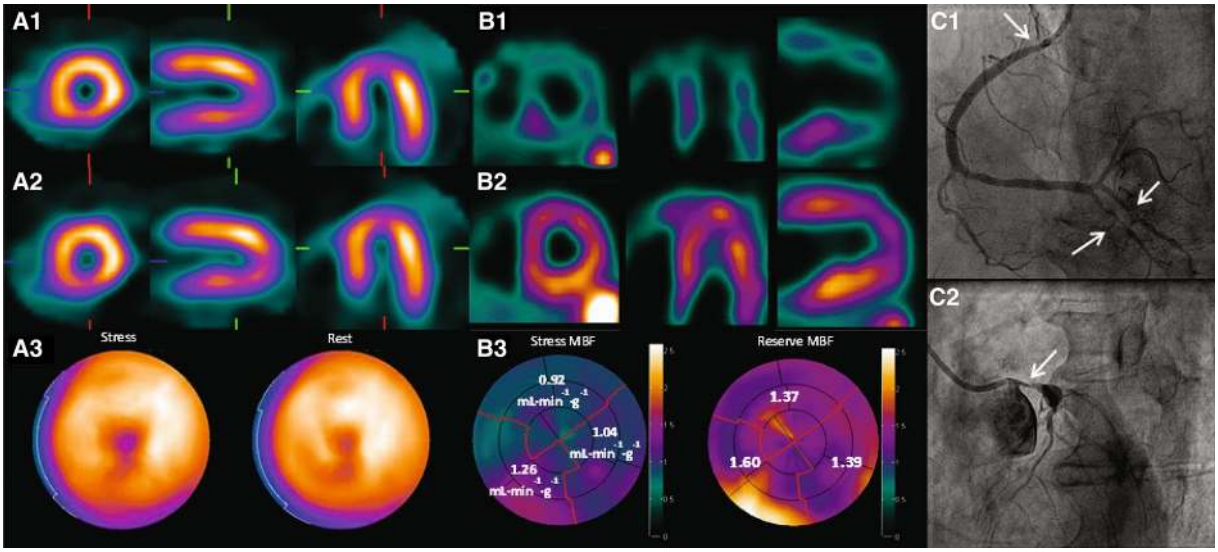

Fig. 3 ^{99m}Tc-Tetrofosmin SPECT (A), $H_2{}^{15}O$ PET (B) and invasive coronary angiography (C) images of a 73-year-old male with chest pain. Short and long axis images during stress (*A1*) and rest (*A2*) show a homogenous tracer distribution indicating a normal perfusion. Stress and rest polarmaps (*A3*) display the same normal perfusion pattern. PET derived short and long axis images show an extensive attenuated perfusion pattern during stress (*B1*) as compared to rest (*B2*). Quantitative MBF values provided in the polarmaps (*B3*) indicate 'balanced ischemia' with impaired hyperemic MBF (<2.30 mL min^{-1} g^{-1}) and flow reserve (<2.50) values in each vascular territory. Invasive coronary angiography confirmed the diagnosis with multi vessel disease located at the proximal and distal right coronary artery (*C1*) and left main coronary artery (*C2*) as indicated with *arrows*

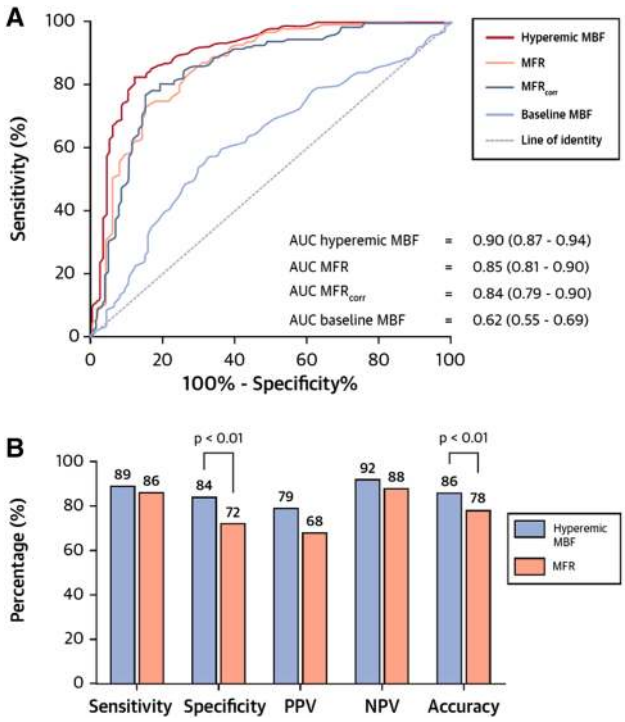

Fig. 4 Diagnostic performance of quantitative PET perfusion parameters. ROC curve analysis with corresponding AUCs and 95% CI displaying the diagnostic performance of hyperemic MBF, MFR, MFRcorr, and baseline MBF for the detection of hemodynamically significant CAD as indicated by FFR on a per patient basis (**a**). Sensitivity, specificity, PPV, NPV, and accuracy on a per patient basis of quantitative PET using hyperemic MBF and MFR, respectively, as a perfusion parameter (**b**). Adapted from Danad et al. [40]

involving 330 patients, reported a sensitivity, specificity, and accuracy of 89, 84, and 86% against 86, 72, and 78% for hyperemic MBF and CFR, respectively [40] (Fig. 4).

Prognostic value of PET imaging

Studies determining the prognostic significance of SPECT contain larger databases, nonetheless parallel the value of PET [55]. The extent and severity of PET derived perfusion defects have also been demonstrated to hold strong prognostic information beyond traditional cardiovascular risk factors [56, 57]. In addition, the quantitative nature of PET has the potential to further increase prognostic significance. Due to greater availability, especially quantitative ^{82}Rb and $^{13}NH_3$ PET have shown incremental value for predicting adverse cardiac events over traditional relative perfusion imaging grading [4, 58–60]. Murthy et al. [4] revealed a significant association between quantitative coronary flow reserve (CFR) measurements and cardiac mortally even after adjustment for traditional risk factors and visual perfusion imaging grading in nearly three thousand patients undergoing ^{82}Rb PET imaging. CFR measurements also induced correct reclassification of estimated risk categories in 35% of patients with a previously intermediate risk on cardiac death. Of particular interest is reclassification of perfusion images with visually homogenous tracer distribution caused by diffusely blunted hyperemic perfusion. Several studies have revealed that this subset of patients is at increased risk for future cardiac events [58, 59, 61, 62] Additionally, reduced flow values predict higher risk of cardiac events, even without obstructive CAD. Microvascular

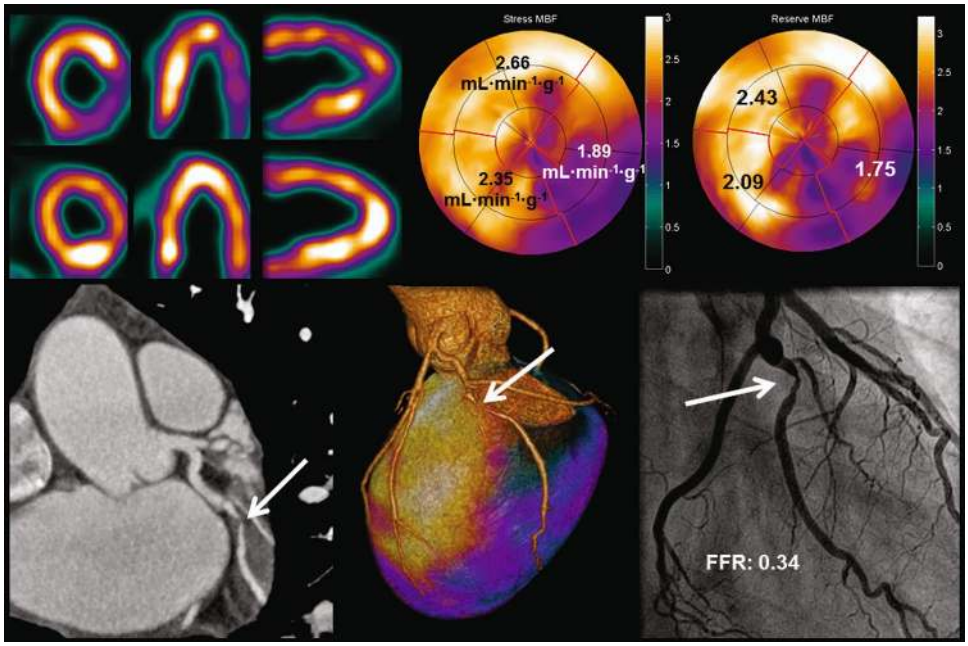

Fig. 5 Case example of a 46-year-old male with typical anginal chest pain. PET showed an inferolateral perfusion defect with an abnormal hyperemic perfusion of 1.89 mL min^{-1} g^{-1} and a myocardial flow reserve of 1.75. CCTA displayed an obstructive soft plaque located in the obtuse marginal branch. Fused PET and CCTA images revealed a perfusion defect downstream from the coronary stenosis. Invasive coronary angiography showed angiographic significant luminal narrowing of the obtuse marginal branch (1-vessel disease) with an FFR of 0.34

dysfunction is thought to play an important pathophysiological role in these patients [63, 64].

Additive value of hybrid PET/CT

Current PET scanners are virtually always equipped with a CT component. These hybrid PET/CT devices are now available up to 128-slice CT and offer near simultaneous assessment of comprehensive anatomical and functional information within a single scanning session, which can be as short as 30 min. An example is shown in Fig. 5.

Coronary computed tomography angiography (CCTA) is an established tool for the non-invasive detection of coronary atherosclerotic stenosis. A multitude of studies have shown a high diagnostic performance of CCTA for the identification of coronary artery stenosis [65–67]. In particular, its sensitivity and negative predictive value are consistently demonstrated to be near perfect, approximating 100%. CCTA is therefore currently the ultimate modality to exclude CAD in patients with a low to intermediate pre-test likelihood of disease. Furthermore, CCTA enables noninvasive evaluation of plaque morphology. Thereby detecting very early stages of CAD as well as plaques that might be vulnerable for rupture [68]. The specificity is, however, hampered as stenosis severity is often overestimated [69]. Another downside of CCTA concerns its limited ability to predict hemodynamic consequences of atherosclerotic stenosis.

On the contrary, myocardial perfusion imaging using either PET or SPECT, is particularly useful to assess hemodynamic significances and thus document myocardial ischemia. As mentioned before, without the knowledge of coronary anatomy and (the location of) stenosis, the results of perfusion imaging should be interpreted carefully.

In summary of the above, either a solely anatomical or functional approach in the evaluation of CAD has its limitations. Therefore, a hybrid assessment could provide complementary rather than overlapping information. The limited number of studies on the diagnostic value of PET/CT seem to confirm the theoretical enhanced accuracy as compared with either modality alone [18, 19, 70, 71]. Other studies revealed analogous improvement of diagnostic performance when fusing SPECT and CCTA [72, 73]. It is shown that especially the moderate specificity of CCTA benefits from the use of hybrid imaging and results in a more judicious referral pattern for invasive coronary angiography [74–76].

In the absence of prognostic data on hybrid PET/CT, the results from hybrid SPECT/CT studies indicate an enhanced risk stratification compared to standalone modalities [75, 77, 78]. This holds particularly true when either perfusion or angiographic imaging exhibit equivocal results. Kim et al. [77] demonstrated incremental prognostic value of sequential SPECT and CCTA in 1295 patients with suspected CAD. However, there was no significant additive value in the case of either stenosis ≥90% on CCTA or SSS ≥ 4 on SPECT. Figure 5 illustrates an example of both standalone modalities as well as hybrid imaging in comparison with invasive coronary angiography.

Interestingly, CT and CMR imaging provide alternative approaches with the possibility of assessing both anatomy and perfusion using a single imaging modality. For CT, the assessment of coronary anatomy can be combined with myocardial perfusion. But the acquisition of such a dynamic first pass sequence comes at the cost of high patient radiation burden, next to the aforementioned unfavorable contrast agent characteristics for CT. A recent multicenter trial, however, showed that CT perfusion using a 320-slice CT scanner improved diagnostic accuracy over CCTA alone [79]. CMR does not have the issue with ionizing radiation and can be combined with e.g. the evaluation of LV and valvular function. In a recent trial, the diagnostic accuracy of CMR in the detection of CAD was found to be superior to SPECT [31]. Still, also CMR perfusion faces multiple technical issues such as imaging artifacts, incomplete coverage of the LV and, as mentioned before, the gadolinium contrast agent impedes accurate MBF measurements with the corresponding disadvantages as compared to PET. Furthermore, not every patient is eligible to undergo CMR because of claustrophobia and contraindications such as pacemakers and implantable cardiac defibrillators.

Conclusion

PET perfusion imaging yields higher image quality and diagnostic accuracy, but lower radiation burden in comparison with SPECT. Using modern PET/CT scanners in combination with appropriate PET radiotracers, absolute quantification can be provided within a single, short scanning protocol. Quantification of flow improves both diagnostic accuracy as well as the prediction of major adverse cardiac events. Promising new PET tracers might increase clinical implementation of PET perfusion in the near future. Furthermore, hybrid PET/CT has shown incremental value compared to either one of the standalone modalities.

Compliance with ethical standards

Conflict of interest The authors have no conflict of interest to declare.

References

1. Genovesi D, Giorgetti A, Gimelli A, Kusch A, D'Aragona T, I, Casagranda M, Cannizzaro G, Giubbini R, Bertagna F, Fagioli G, Rossi M, Romeo A, Bertolaccini P, Bonini R, Marzullo P (2011) Impact of attenuation correction and gated acquisition in SPECT myocardial perfusion imaging: results of the multicentre SPAG (SPECT Attenuation Correction vs Gated) study. Eur J Nucl Med Mol Imaging 38:1890–1898
2. Slomka P, Berman DS, Germano G (2016) Myocardial blood flow from SPECT. J Nucl Cardiol 24:278–281
3. Knaapen P, Lubberink M (2008) Cardiac positron emission tomography: myocardial perfusion and metabolism in clinical practice. Clin Res Cardiol 97:791–796
4. Murthy VL, Naya M, Foster CR, Hainer J, Gaber M, Di CG, Blankstein R, Dorbala S, Sitek A, Pencina MJ, Di Carli MF (2011) Improved cardiac risk assessment with noninvasive measures of coronary flow reserve. Circulation 124:2215–2224
5. Gould KL, Johnson NP, Bateman TM, Beanlands RS, Bengel FM, Bober R, Camici PG, Cerqueira MD, Chow BJ, Di Carli MF, Dorbala S, Gewirtz H, Gropler RJ, Kaufmann PA, Knaapen P, Knuuti J, Merhige ME, Rentrop KP, Ruddy TD, Schelbert HR, Schindler TH, Schwaiger M, Sdringola S, Vitarello J, Williams KA Sr, Gordon D, Dilsizian V, Narula J (2013) Anatomic versus physiologic assessment of coronary artery disease. Role of coronary flow reserve, fractional flow reserve, and positron emission tomography imaging in revascularization decision-making. J Am Coll Cardiol 62:1639–1653
6. Schindler TH, Schelbert HR, Quercioli A, Dilsizian V (2010) Cardiac PET imaging for the detection and monitoring of coronary artery disease and microvascular health. JACC 3:623–640
7. Maddahi J, Packard RR (2014) Cardiac PET perfusion tracers: current status and future directions. Semin Nucl Med 44:333–343
8. Rischpler C, Park MJ, Fung GS, Javadi M, Tsui BM, Higuchi T (2012) Advances in PET myocardial perfusion imaging: F-18 labeled tracers. Ann Nucl Med 26:1–6
9. Huisman MC, Higuchi T, Reder S, Nekolla SG, Poethko T, Wester HJ, Ziegler SI, Casebier DS, Robinson SP, Schwaiger M (2008) Initial characterization of an ^{18}F-labeled myocardial perfusion tracer. J Nucl Med 49:630–636
10. Iida H, Kanno I, Takahashi A, Miura S, Murakami M, Takahashi K, Ono Y, Shishido F, Inugami A, Tomura N (1988) Measurement of absolute myocardial blood flow with $H_2{}^{15}O$ and dynamic positron-emission tomography. Strategy for quantification in relation to the partial-volume effect. Circulation 78:104–115
11. Huang SC, Williams BA, Krivokapich J, Araujo L, Phelps ME, Schelbert HR (1989) Rabbit myocardial ^{82}Rb kinetics and a compartmental model for blood flow estimation. Am J Physiol 256:H1156–H1164
12. Schelbert HR, Phelps ME, Huang SC, MacDonald NS, Hansen H, Selin C, Kuhl DE (1981) N-13 ammonia as an indicator of myocardial blood flow. Circulation 63:1259–1272
13. Yalamanchili P, Wexler E, Hayes M, Yu M, Bozek J, Kagan M, Radeke HS, Azure M, Purohit A, Casebier DS, Robinson SP (2007) Mechanism of uptake and retention of F-18 BMS-747158-02 in cardiomyocytes: a novel PET myocardial imaging agent. J Nucl Cardiol 14:782–788
14. Khorsand A, Graf S, Eidherr H, Wadsak W, Kletter K, Sochor H, Schuster E, Porenta G (2005) Gated cardiac ^{13}N-NH_3 PET for assessment of left ventricular volumes, mass, and ejection fraction: comparison with electrocardiography-gated 18F-FDG PET. J Nucl Med 46:2009–2013
15. Di Carli MF, Hachamovitch R (2007) New technology for noninvasive evaluation of coronary artery disease. Circulation 115:1464–1480
16. Harms HJ, Knaapen P, de Haan S, Halbmeijer R, Lammertsma AA, Lubberink M (2011) Automatic generation of absolute myocardial blood flow images using [^{15}O]H_2O and a clinical PET/CT scanner. Eur J Nucl Med Mol Imaging 38:930–939
17. Nesterov SV, Han C, Maki M, Kajander S, Naum AG, Helenius H, Lisinen I, Ukkonen H, Pietila M, Joutsiniemi E, Knuuti J (2009) Myocardial perfusion quantitation with ^{15}O-labelled water PET: high reproducibility of the new cardiac analysis software (Carimas). Eur J Nucl Med Mol Imaging 36:1594–1602
18. Danad I, Raijmakers PG, Appelman YE, Harms HJ, de HS, van den Oever ML, Heymans MW, Tulevski II, van KC, Hoekstra OS, Lammertsma AA, Lubberink M, van Rossum AC, Knaapen P (2013) Hybrid imaging using quantitative $H_2{}^{15}O$ PET and CT-based coronary angiography for the detection of coronary artery disease. J Nucl Med 54:55–63
19. Kajander S, Joutsiniemi E, Saraste M, Pietila M, Ukkonen H, Saraste A, Sipila HT, Teras M, Maki M, Airaksinen J, Hartiala J, Knuuti J (2010) Cardiac positron emission tomography/computed tomography imaging accurately detects anatomically and functionally significant coronary artery disease. Circulation 122:603–613
20. Maddahi J (2012) Properties of an ideal PET perfusion tracer: new PET tracer cases and data. J Nucl Cardiol 19(Suppl 1):S30–S37
21. Bergmann SR, Fox KA, Rand AL, McElvany KD, Welch MJ, Markham J, Sobel BE (1984) Quantification of regional myocardial blood flow in vivo with $H_2{}^{15}O$. Circulation 70:724–733
22. Saraste A, Kajander S, Han C, Nesterov SV, Knuuti J (2012) PET: is myocardial flow quantification a clinical reality? J Nucl Cardiol 19:1044–1059
23. Bol A, Melin JA, Vanoverschelde JL, Baudhuin T, Vogelaers D, De PM, Michel C, Luxen A, Labar D, Cogneau M (1993) Direct comparison of [^{13}N]ammonia and [^{15}O]water estimates of perfusion with quantification of regional myocardial blood flow by microspheres. Circulation 87:512–525
24. Kaufmann PA, Gnecchi-Ruscone T, Yap JT, Rimoldi O, Camici PG (1999) Assessment of the reproducibility of baseline and hyperemic myocardial blood flow measurements with ^{15}O-labeled water and PET. J Nucl Med 40:1848–1856
25. Hutchins GD, Schwaiger M, Rosenspire KC, Krivokapich J, Schelbert H, Kuhl DE (1990) Noninvasive quantification of regional blood flow in the human heart using N-13 ammonia and dynamic positron emission tomographic imaging. J Am Coll Cardiol 15:1032–1042
26. deKemp RA, Declerck J, Klein R, Pan XB, Nakazato R, Tonge C, Arumugam P, Berman DS, Germano G, Beanlands RS, Slomka PJ (2013) Multisoftware reproducibility study of stress and rest myocardial blood flow assessed with 3D dynamic PET/CT and a 1-tissue-compartment model of ^{82}Rb kinetics. J Nucl Med 54:571–577
27. Slomka PJ, Alexanderson E, Jacome R, Jimenez M, Romero E, Meave A, Le ML, Dalhbom M, Berman DS, Germano G, Schelbert H (2012) Comparison of clinical tools for measurements of regional stress and rest myocardial blood flow assessed with ^{13}N-ammonia PET/CT. J Nucl Med 53:171–181
28. Lautamaki R, George RT, Kitagawa K, Higuchi T, Merrill J, Voicu C, DiPaula A, Nekolla SG, Lima JA, Lardo AC, Bengel

FM (2009) Rubidium-82 PET-CT for quantitative assessment of myocardial blood flow: validation in a canine model of coronary artery stenosis. Eur J Nucl Med Mol Imaging 36:576–586
29. Nekolla SG, Reder S, Saraste A, Higuchi T, Dzewas G, Preissel A, Huisman M, Poethko T, Schuster T, Yu M, Robinson S, Casebier D, Henke J, Wester HJ, Schwaiger M (2009) Evaluation of the novel myocardial perfusion positron-emission tomography tracer 18F-BMS-747158-02: comparison to ^{13}N-ammonia and validation with microspheres in a pig model. Circulation 119:2333–2342
30. Danad I, Raijmakers PG, Knaapen P (2013) Diagnosing coronary artery disease with hybrid PET/CT: it takes two to tango. J Nucl Cardiol 20:874–890
31. Greenwood JP, Maredia N, Younger JF, Brown JM, Nixon J, Everett CC, Bijsterveld P, Ridgway JP, Radjenovic A, Dickinson CJ, Ball SG, Plein S (2012) Cardiovascular magnetic resonance and single-photon emission computed tomography for diagnosis of coronary heart disease (CE-MARC): a prospective trial. Lancet 379:453–460
32. Blankstein R, Shturman LD, Rogers IS, Rocha-Filho JA, Okada DR, Sarwar A, Soni AV, Bezerra H, Ghoshhajra BB, Petranovic M, Loureiro R, Feuchtner G, Gewirtz H, Hoffmann U, Mamuya WS, Brady TJ, Cury RC (2009) Adenosine-induced stress myocardial perfusion imaging using dual-source cardiac computed tomography. J Am Coll Cardiol 54:1072–1084
33. Klocke FJ, Baird MG, Lorell BH, Bateman TM, Messer JV, Berman DS, O'Gara PT, Carabello BA, Russell RO Jr, Cerqueira MD, St John Sutton MG, DeMaria AN, Udelson JE, Kennedy JW, Verani MS, Williams KA, Antman EM, Smith SC Jr, Alpert JS, Gregoratos G, Anderson JL, Hiratzka LF, Faxon DP, Hunt SA, Fuster V, Jacobs AK, Gibbons RJ, Russell RO (2003) ACC/AHA/ASNC guidelines for the clinical use of cardiac radionuclide imaging—executive summary: a report of the American College of Cardiology/American Heart Association Task Force on Practice Guidelines (ACC/AHA/ASNC Committee to Revise the 1995 Guidelines for the Clinical Use of Cardiac Radionuclide Imaging). J Am Coll Cardiol 42:1318–1333
34. Verberne HJ, Acampa W, Anagnostopoulos C, Ballinger J, Bengel F, De BP, Buechel RR, Cuocolo A, van Eck-Smit BL, Flotats A, Hacker M, Hindorf C, Kaufmann PA, Lindner O, Ljungberg M, Lonsdale M, Manrique A, Minarik D, Scholte AJ, Slart RH, Tragardh E, de Wit TC, Hesse B (2015) EANM procedural guidelines for radionuclide myocardial perfusion imaging with SPECT and SPECT/CT: 2015 revision. Eur J Nucl Med Mol Imaging 42:1929–1940
35. Anagnostopoulos C, Georgakopoulos A, Pianou N, Nekolla SG (2013) Assessment of myocardial perfusion and viability by positron emission tomography. Int J Cardiol 167:1737–1749
36. Danad I, Raijmakers PG, Appelman YE, Harms HJ, de HS, van den Oever ML, van KC, Allaart CP, Hoekstra OS, Lammertsma AA, Lubberink M, van Rossum AC, Knaapen P (2012) Coronary risk factors and myocardial blood flow in patients evaluated for coronary artery disease: a quantitative [^{15}O]H_2O PET/CT study. Eur J Nucl Med Mol Imaging 39:102–112
37. Chareonthaitawee P, Kaufmann PA, Rimoldi O, Camici PG (2001) Heterogeneity of resting and hyperemic myocardial blood flow in healthy humans. Cardiovasc Res 50:151–161
38. Laaksonen MS, Kalliokoski KK, Luotolahti M, Kemppainen J, Teras M, Kyrolainen H, Nuutila P, Knuuti J (2007) Myocardial perfusion during exercise in endurance-trained and untrained humans. Am J Physiol Regul Integr Comp Physiol 293:R837–R843
39. Sdringola S, Johnson NP, Kirkeeide RL, Cid E, Gould KL (2011) Impact of unexpected factors on quantitative myocardial perfusion and coronary flow reserve in young, asymptomatic volunteers. JACC 4:402–412
40. Danad I, Uusitalo V, Kero T, Saraste A, Raijmakers PG, Lammertsma AA, Heymans MW, Kajander SA, Pietila M, James S, Sorensen J, Knaapen P, Knuuti J (2014) Quantitative assessment of myocardial perfusion in the detection of significant coronary artery disease: cutoff values and diagnostic accuracy of quantitative [$^{(15)}$O]H_2O PET imaging. J Am Coll Cardiol 64:1464–1475
41. Majmudar MD, Murthy VL, Shah RV, Kolli S, Mousavi N, Foster CR, Hainer J, Blankstein R, Dorbala S, Sitek A, Stevenson LW, Mehra MR, Di Carli MF (2015) Quantification of coronary flow reserve in patients with ischaemic and non-ischaemic cardiomyopathy and its association with clinical outcomes. Eur Heart J Cardiovasc Imaging 16:900–909
42. Jaarsma C, Leiner T, Bekkers SC, Crijns HJ, Wildberger JE, Nagel E, Nelemans PJ, Schalla S (2012) Diagnostic performance of noninvasive myocardial perfusion imaging using single-photon emission computed tomography, cardiac magnetic resonance, and positron emission tomography imaging for the detection of obstructive coronary artery disease: a meta-analysis. J Am Coll Cardiol 59:1719–1728
43. Mc Ardle BA, Dowsley TF, deKemp RA, Wells GA, Beanlands RS (2012) Does rubidium-82 PET have superior accuracy to SPECT perfusion imaging for the diagnosis of obstructive coronary disease?: A systematic review and meta-analysis. J Am Coll Cardiol 60:1828–1837
44. Takx RA, Blomberg BA, El AH, Habets J, de Jong PA, Nagel E, Hoffmann U, Leiner T (2015) Diagnostic accuracy of stress myocardial perfusion imaging compared to invasive coronary angiography with fractional flow reserve meta-analysis. Circulation 8:e002666
45. Yoshinaga K, Katoh C, Manabe O, Klein R, Naya M, Sakakibara M, Yamada S, deKemp RA, Tsutsui H, Tamaki N (2011) Incremental diagnostic value of regional myocardial blood flow quantification over relative perfusion imaging with generator-produced rubidium-82 PET. Circ J 75:2628–2634
46. Muzik O, Duvernoy C, Beanlands RS, Sawada S, Dayanikli F, Wolfe ER Jr, Schwaiger M (1998) Assessment of diagnostic performance of quantitative flow measurements in normal subjects and patients with angiographically documented coronary artery disease by means of nitrogen-13 ammonia and positron emission tomography. J Am Coll Cardiol 31:534–540
47. Hajjiri MM, Leavitt MB, Zheng H, Spooner AE, Fischman AJ, Gewirtz H (2009) Comparison of positron emission tomography measurement of adenosine-stimulated absolute myocardial blood flow versus relative myocardial tracer content for physiological assessment of coronary artery stenosis severity and location. JACC 2:751–758
48. Kajander SA, Joutsiniemi E, Saraste M, Pietila M, Ukkonen H, Saraste A, Sipila HT, Teras M, Maki M, Airaksinen J, Hartiala J, Knuuti J (2011) Clinical value of absolute quantification of myocardial perfusion with $^{(15)}$O-water in coronary artery disease. Circ Cardiovasc Imaging 4:678–684
49. Fiechter M, Ghadri JR, Gebhard C, Fuchs TA, Pazhenkottil AP, Nkoulou RN, Herzog BA, Wyss CA, Gaemperli O, Kaufmann PA (2012) Diagnostic value of ^{13}N-ammonia myocardial perfusion PET: added value of myocardial flow reserve. J Nucl Med 53:1230–1234
50. Ziadi MC, deKemp RA, Williams K, Guo A, Renaud JM, Chow BJ, Klein R, Ruddy TD, Aung M, Garrard L, Beanlands RS (2012) Does quantification of myocardial flow reserve using rubidium-82 positron emission tomography facilitate detection of multivessel coronary artery disease? J Nucl Cardiol 19:670–680
51. Dorbala S, Hachamovitch R, Curillova Z, Thomas D, Vangala D, Kwong RY, Di Carli MF (2009) Incremental prognostic value of gated Rb-82 positron emission tomography myocardial perfusion imaging over clinical variables and rest LVEF. JACC 2:846–854

52. Rischpler C, Higuchi T, Fukushima K, Javadi MS, Merrill J, Nekolla SG, Bravo PE, Bengel FM (2012) Transient ischemic dilation ratio in ^{82}Rb PET myocardial perfusion imaging: normal values and significance as a diagnostic and prognostic marker. J Nucl Med 53:723–730
53. Joutsiniemi E, Saraste A, Pietila M, Maki M, Kajander S, Ukkonen H, Airaksinen J, Knuuti J (2014) Absolute flow or myocardial flow reserve for the detection of significant coronary artery disease? Eur Heart J Cardiovasc Imaging 15:659–665
54. Danad I, Raijmakers PG, Harms HJ, Heymans MW, van Royen N, Lubberink M, Boellaard R, van Rossum AC, Lammertsma AA, Knaapen P (2014) Impact of anatomical and functional severity of coronary atherosclerotic plaques on the transmural perfusion gradient: a [^{15}O]H_2O PET study. Eur Heart J 35:2094–2105
55. Hachamovitch R, Berman DS, Shaw LJ, Kiat H, Cohen I, Cabico JA, Friedman J, Diamond GA (1998) Incremental prognostic value of myocardial perfusion single photon emission computed tomography for the prediction of cardiac death: differential stratification for risk of cardiac death and myocardial infarction. Circulation 97:535–543
56. Dorbala S, Di Carli MF, Beanlands RS, Merhige ME, Williams BA, Veledar E, Chow BJW, Min JK, Pencina MJ, Berman DS, Shaw LJ (2013) Prognostic value of stress myocardial perfusion positron emission tomography: results from a multicenter observational registry. J Am Coll Cardiol 61:176–184
57. Yoshinaga K, Chow BJ, Williams K, Chen L, deKemp RA, Garrard L, Lok-Tin SA, Aung M, Davies RA, Ruddy TD, Beanlands RS (2006) What is the prognostic value of myocardial perfusion imaging using rubidium-82 positron emission tomography? J Am Coll Cardiol 48:1029–1039
58. Herzog BA, Husmann L, Valenta I, Gaemperli O, Siegrist PT, Tay FM, Burkhard N, Wyss CA, Kaufmann PA (2009) Long-term prognostic value of ^{13}N-ammonia myocardial perfusion positron emission tomography added value of coronary flow reserve. J Am Coll Cardiol 54:150–156
59. Ziadi MC, deKemp RA, Williams KA, Guo A, Chow BJ, Renaud JM, Ruddy TD, Sarveswaran N, Tee RE, Beanlands RS (2011) Impaired myocardial flow reserve on rubidium-82 positron emission tomography imaging predicts adverse outcomes in patients assessed for myocardial ischemia. J Am Coll Cardiol 58:740–748
60. Taqueti VR, Hachamovitch R, Murthy VL, Naya M, Foster CR, Hainer J, Dorbala S, Blankstein R, Di Carli MF (2015) Global coronary flow reserve is associated with adverse cardiovascular events independently of luminal angiographic severity and modifies the effect of early revascularization. Circulation 131:19–27
61. Fukushima K, Javadi MS, Higuchi T, Lautamaki R, Merrill J, Nekolla SG, Bengel FM (2011) Prediction of short-term cardiovascular events using quantification of global myocardial flow reserve in patients referred for clinical ^{82}Rb PET perfusion imaging. J Nucl Med 52:726–732
62. Farhad H, Dunet V, Bachelard K, Allenbach G, Kaufmann PA, Prior JO (2013) Added prognostic value of myocardial blood flow quantitation in rubidium-82 positron emission tomography imaging. Eur Heart J Cardiovasc Imaging 14:1203–1210
63. Taqueti VR, Everett BM, Murthy VL, Gaber M, Foster CR, Hainer J, Blankstein R, Dorbala S, Di Carli MF (2015) Interaction of impaired coronary flow reserve and cardiomyocyte injury on adverse cardiovascular outcomes in patients without overt coronary artery disease. Circulation 131:528–535
64. Lee JM, Jung JH, Hwang D, Park J, Fan Y, Na SH, Doh JH, Nam CW, Shin ES, Koo BK (2016) Coronary flow reserve and microcirculatory resistance in patients with intermediate coronary stenosis. J Am Coll Cardiol 67:1158–1169
65. Meijboom WB, Meijs MF, Schuijf JD, Cramer MJ, Mollet NR, van Mieghem CA, Nieman K, van Werkhoven JM, Pundziute G, Weustink AC, de Vos AM, Pugliese F, Rensing B, Jukema JW, Bax JJ, Prokop M, Doevendans PA, Hunink MG, Krestin GP, de Feyter PJ (2008) Diagnostic accuracy of 64-slice computed tomography coronary angiography: a prospective, multicenter, multivendor study. J Am Coll Cardiol 52:2135–2144
66. Budoff MJ, Dowe D, Jollis JG, Gitter M, Sutherland J, Halamert E, Scherer M, Bellinger R, Martin A, Benton R, Delago A, Min JK (2008) Diagnostic performance of 64-multidetector row coronary computed tomographic angiography for evaluation of coronary artery stenosis in individuals without known coronary artery disease: results from the prospective multicenter ACCURACY (Assessment by Coronary Computed Tomographic Angiography of Individuals Undergoing Invasive Coronary Angiography) trial. J Am Coll Cardiol 52:1724–1732
67. Shaw LJ, Hausleiter J, Achenbach S, Al-Mallah M, Berman DS, Budoff MJ, Cademartiri F, Callister TQ, Chang HJ, Kim YJ, Cheng VY, Chow BJ, Cury RC, Delago AJ, Dunning AL, Feuchtner GM, Hadamitzky M, Karlsberg RP, Kaufmann PA, Leipsic J, Lin FY, Chinnaiyan KM, Maffei E, Raff GL, Villines TC, Labounty T, Gomez MJ, Min JK (2012) Coronary computed tomographic angiography as a gatekeeper to invasive diagnostic and surgical procedures: results from the multicenter CONFIRM (Coronary CT Angiography Evaluation for Clinical Outcomes: an International Multicenter) registry. J Am Coll Cardiol 60:2103–2114
68. Motoyama S, Ito H, Sarai M, Kondo T, Kawai H, Nagahara Y, Harigaya H, Kan S, Anno H, Takahashi H, Naruse H, Ishii J, Hecht H, Shaw LJ, Ozaki Y, Narula J (2015) Plaque characterization by coronary computed tomography angiography and the likelihood of acute coronary events in mid-term follow-up. J Am Coll Cardiol 66:337–346
69. Schroeder S, Achenbach S, Bengel F, Burgstahler C, Cademartiri F, de FP, George R, Kaufmann P, Kopp AF, Knuuti J, Ropers D, Schuijf J, Tops LF, Bax JJ (2008) Cardiac computed tomography: indications, applications, limitations, and training requirements: report of a Writing Group deployed by the Working Group Nuclear Cardiology and Cardiac CT of the European Society of Cardiology and the European Council of Nuclear Cardiology. Eur Heart J 29:531–556
70. Groves AM, Speechly-Dick ME, Kayani I, Pugliese F, Endozo R, McEwan J, Menezes LJ, Habib SB, Prvulovich E, Ell PJ (2009) First experience of combined cardiac PET/64-detector CT angiography with invasive angiographic validation. Eur J Nucl Med Mol Imaging 36:2027–2033
71. Thomassen A, Petersen H, Diederichsen AC, Mickley H, Jensen LO, Johansen A, Gerke O, Braad PE, Thayssen P, Hoilund-Carlsen MM, Vach W, Knuuti J, Hoilund-Carlsen PF (2013) Hybrid CT angiography and quantitative ^{15}O-water PET for assessment of coronary artery disease: comparison with quantitative coronary angiography. Eur J Nucl Med Mol Imaging 40:1894–1904
72. Rispler S, Keidar Z, Ghersin E, Roguin A, Soil A, Dragu R, Litmanovich D, Frenkel A, Aronson D, Engel A, Beyar R, Israel O (2007) Integrated single-photon emission computed tomography and computed tomography coronary angiography for the assessment of hemodynamically significant coronary artery lesions. J Am Coll Cardiol 49:1059–1067
73. Schaap J, de Groot JA, Nieman K, Meijboom WB, Boekholdt SM, Kauling RM, Post MC, Van der Heyden JA, de Kroon TL, Rensing BJ, Moons KG, Verzijlbergen JF (2014) Added value of hybrid myocardial perfusion SPECT and CT coronary angiography in the diagnosis of coronary artery disease. Eur Heart J Cardiovasc Imaging 15:1281–1288

74. Danad I, Raijmakers PG, Harms HJ, van KC, van RN, Diamant M, Lammertsma AA, Lubberink M, van Rossum AC, Knaapen P (2014) Effect of cardiac hybrid (1)(5)O-water PET/CT imaging on downstream referral for invasive coronary angiography and revascularization rate. Eur Heart J Cardiovasc Imaging 15:170–179
75. Pazhenkottil AP, Nkoulou RN, Ghadri JR, Herzog BA, Kuest SM, Husmann L, Wolfrum M, Goetti R, Buechel RR, Gaemperli O, Luscher TF, Kaufmann PA (2011) Impact of cardiac hybrid single-photon emission computed tomography/computed tomography imaging on choice of treatment strategy in coronary artery disease. Eur Heart J 32:2824–2829
76. Schaap J, de Groot JA, Nieman K, Meijboom WB, Boekholdt SM, Post MC, Van der Heyden JA, de Kroon TL, Rensing BJ, Moons KG, Verzijlbergen JF (2013) Hybrid myocardial perfusion SPECT/CT coronary angiography and invasive coronary angiography in patients with stable angina pectoris lead to similar treatment decisions. Heart 99:188–194
77. Kim HL, Kim YJ, Lee SP, Park EA, Paeng JC, Kim HK, Lee W, Cho GY, Zo JH, Choi DJ, Sohn DW (2014) Incremental prognostic value of sequential imaging of single-photon emission computed tomography and coronary computed tomography angiography in patients with suspected coronary artery disease. Eur Heart J Cardiovasc Imaging 15:878–885
78. van Werkhoven JM, Schuijf JD, Gaemperli O, Jukema JW, Boersma E, Wijns W, Stolzmann P, Alkadhi H, Valenta I, Stokkel MP, Kroft LJ, de RA, Pundziute G, Scholte A, van der Wall EE, Kaufmann PA, Bax JJ (2009) Prognostic value of multislice computed tomography and gated single-photon emission computed tomography in patients with suspected coronary artery disease. J Am Coll Cardiol 53:623–632
79. Rochitte CE, George RT, Chen MY, Arbab-Zadeh A, Dewey M, Miller JM, Niinuma H, Yoshioka K, Kitagawa K, Nakamori S, Laham R, Vavere AL, Cerci RJ, Mehra VC, Nomura C, Kofoed KF, Jinzaki M, Kuribayashi S, de RA, Laule M, Tan SY, Hoe J, Paul N, Rybicki FJ, Brinker JA, Arai AE, Cox C, Clouse ME, Di Carli MF, Lima JA (2014) Computed tomography angiography and perfusion to assess coronary artery stenosis causing perfusion defects by single photon emission computed tomography: the CORE320 study. Eur Heart J 35:1120–1130